

Turbodrill Design and Performance Analysis

A. Mokaramian^{1†}, V. Rasouli¹ and G. Cavanough²

¹ *Deep Exploration Technologies Cooperative Research Centre (DET CRC) and Department of Petroleum Engineering, Curtin University, Perth, WA 6151, Australia*

² *Deep Exploration Technologies Cooperative Research Centre (DET CRC), and CSIRO, Queensland Centre for Advanced Technologies (QCAT), Brisbane, Q 4069, Australia*

†Corresponding Author Email: amir.mokaramian@postgrad.curtin.edu.au

(Received September 01, 2012; accepted June 10, 2014)

ABSTRACT

Turbodrill (turbine down hole motor) has been recently proposed by the authors as the preferred drive mechanism with high rotation speed for hard rocks drilling for deep mineral exploration applications. Turbodrill is a type of hydraulic axial turbomachinery in which turbine motor section has multistage of rotors and stators that convert the hydraulic power provided by the drilling fluid to mechanical power with diverting the fluid flow through the stator vanes to rotor vanes. This paper presents a methodology for designing multistage turbodrills with asymmetric rotor and stator blades configurations. The numerical simulation approach and the simulation results carried out using computational fluid dynamics (CFD) code for the proposed small size model of turbodrill stage with different drilling fluid (mud) types and various mass flow rates are presented. As a result optimum operational parameters are proposed for gaining the required rotation speed and torque for hard rocks drilling.

Keywords: Hydraulic Turbodrill; Turbine down hole motor; Coiled Tube (CT) drilling; Computational Fluid Dynamics (CFD); Numerical Simulation.

1. INTRODUCTION

Coiled Tube (CT) Turbodrilling technology has been recently proposed for drilling deep hard rocks for mineral exploration applications, Mokaramian et al. (2012). Coiled Tube (CT) is a continuous length of ductile steel or carbon fiber tube that is stored and transported over a large reel (see Fig. 1). The CT Unit (CTU) consists of four basic elements: 1) Reel, for storage and transport of the CT, 2) Injector Head, to provide the surface drive force to run and retrieve the CT, 3) Control Cabin, from which the equipment operator monitors and controls the CT, and 4) Power Pack, to generate hydraulic and pneumatic power required to operate the CT unit. In mineral exploration, drilling small size holes as fast as possible and obtaining reliable samples to the surface yields several advantages over conventional drilling methods. Coiled tube (CT) allows fast drilling by eliminating the connection time and providing continuous circulation during drilling. This enables quick access to the zone of interest to collect the cuttings or obtain core samples.

Coiled tube itself cannot rotate and therefore a down hole motor is needed to provide mechanical power and rotation to the bit. There are many special design criteria to be considered for

successful operation of down hole motors in CT drilling (Beaton and Seale. 2004; RIO 2004; IT 2007). One major concern is that it is often difficult to produce enough weight on bit (WOB) to maximize the rate of penetration (ROP) for optimized drilling. Since the ROP of a fixed cutter drill bit is a product of the depth of cut (DOC) and the rotation speed and because the DOC is primarily produced by the available WOB, in an environment where WOB is limited (as with CT drilling); high rotation speed is the key driver for ROP, Beaton and Seale (2004). Amongst available down hole motors, turbodrills (turbine motors) are the best choice to be used for small size CT drilling hard rocks, Mokaramian et al. (2012); this results in a smooth borehole with little vibrational effects during drilling and produce a high quality hole. The turbine motor section has multistage of stators and rotors which converts the hydraulic power provided by the drilling fluid (pumped from surface) to mechanical power with diverting the fluid flow through the stator vanes to rotor vanes. The fluid will run through the turbodrill and the bit nozzles to cool the bit and remove the cuttings generated under the bit. It will finally carry the cuttings inside the annulus between CT and the hole to the surface.

2. TURBODRILL CHARA CTERISTICS

In general, the down hole turbine motor (Turbo-drill) is composed of two sections: turbine motor section and bearing section i.e. thrust-bearing and radial support bearing, Eskin and Maurer (1997). Figure 2 shows a typical Turbo-drill assembly and the fluid flow path

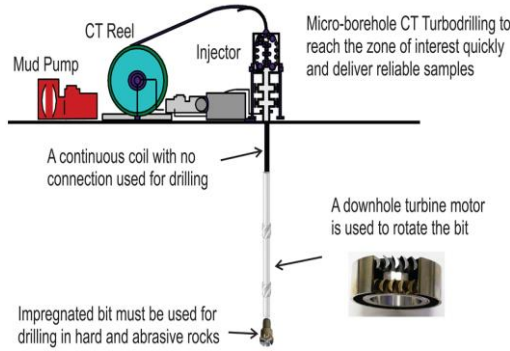


Fig. 1. Schematic of the coiled tubing unit for hard rocks mineral exploration drilling.

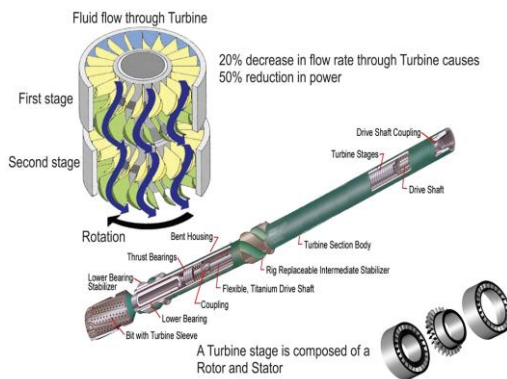


Fig. 2. Turbo-drill assembly and schematic fluid flow through turbine stages, after Beaton and Seale (2004).

through turbine stages. The turbine motor section has multistage of rotors and stators and plurality of rotor and stator vanes on each rotor and stator.

The activating drilling fluid is pumped at high velocity through the motor section, which, because of the vane angle of each rotor and stator (one stage), causes the rotor to rotate the shaft of the motor which is connected to the bit. The energy required to change the rotational direction of the drilling fluid is transformed into rotational and axial (thrust) force. This energy transfer is seen as a pressure drop in the drilling fluid. The thrust is typically absorbed by thrust bearing. The rotational force causes the rotor to rotate relative to the housing. In practice, multiple stages are stacked coaxially until the desired power and torque is achieved.

The primary role of the stator is to swirl the drilling fluid prior to entering the rotor. At the same time, the pressure drop across the stator should be minimized because it increases the pressure

required to pump the drilling fluid. Due to the fact that the stator is rotationally fixed relative to the housing of the turbo-drill, any rotational force generated is absorbed by the housing and is therefore wasted. The primary role of the rotor is to transform the energy of the drilling fluid into rotational energy for rotating the drill bit. This is achieved by changing the direction of the fluid flow. The force required to turn the fluid causes a reaction force on the rotor vanes resulting in turning the rotor.

The main operating parameters that dictate the size of the turbine motors are torque, speed, and mud weight, Sanchez *et al.* (1996). Due to hydrodynamics function, the output power of a turbine motor is not linear with the mud flow rate and 20% decrease in the mass flow rate causes a 50% reduction in the turbine motor output power, Reich *et al.* (2000). A turbine device has the unique characteristic that it will allow mud circulation independent of what torque or power the motor is producing. If the turbine motor is lifted off the bottom of the borehole and mud circulation continues, the motor will speed up to the runaway speed. In this situation the motor produces no drilling torque or power. As the turbine motor is lowered and weight is placed on the motor and thus the bit, the motor begins to slow its speed and produce torque and power. When sufficient weight has been placed on the turbine motor, the motor will produce its maximum possible power. If more weight is added to the turbine motor and the bit, the motor speed and power output will continue to decrease and torque continuously will increase till the motor cease to rotate and the motor is described as being stalled, Lyons and Plisga (2005). At this condition, the turbine motor produces its maximum possible torque. Even when the motor is stalled, the drilling fluid is still circulating.

It is almost impossible to determine formulae for turbines under working conditions, Eskin and Maurer (1997). Laboratory experiments using drilling dynamometer test stand have to be conducted to determine nominal data on Turbo-drills. If the performance parameters for a turbine motor design are known for a given circulation flow rate and mud weight, the performance parameters for other circulation flow rate and mud weight can be found using the following mathematical relationships, Eskin and Maurer (1997):

$$N \propto Q; T \propto Q^2; \Delta p \propto Q^2; P \propto Q^3; \eta \propto \frac{1}{Q}, \quad (1)$$

$$N \propto \frac{1}{\rho}; T \propto \rho; \Delta p \propto \rho; P \propto \rho; \eta \propto \frac{1}{\rho}, \quad (2)$$

where:

N = Turbo-drill output rotation speed (revolution per minute),

ρ = Drilling fluid (mud) density,

P = Turbo-drill output power,

T = Turbo-drill output Torque,

Q = Flow rate,
 Δp = Turbodrill differential pressure,
 η = Turbodrill efficiency.

Depending on the skills of the turbodrill operator the speed may vary from zero rpm to the runaway speed. The turbine motor instantaneous torque T (N.m) for any rotation speed N (rpm) is:

$$T = T_s \left(1 - \frac{N}{N_r} \right) \quad (3)$$

where:
 T_s = Stalled torque (maximum torque),
 N_r = Runaway rotation speed (maximum speed).

The maximum turbine motor power is at the optimum speed, N_o , which is one-half of the runaway speed. This is:

$$N_o = \frac{N_r}{2} \quad (4)$$

The torque at the optimum speed T_o is one-half the stall torque. Thus:

$$T_o = \frac{T_s}{2} \quad (5)$$

Many new turbodrill designs and modifications are currently underway to extend the applicability of Turbodrilling to coiled tubing operations (Radtke et al. 2011, Grigor et al. 2008, Seale et al. 2004). One of the most significant developments in progress is the creation of a turbodrill that is much shorter than existing designs in order to enhance compatibility with coiled tube equipment. Other developments currently underway to improve the compatibility with CT drilling applications include specially designed turbine blades for such applications. These blades are designed to maximize the power output in the shortest possible tool configurations.

3. TURBODRILL DESIGN

When designing a hydraulic multistage turbine, it is assumed that each turbine stage is identical and that the flow rate, pressure drop, rotary speed, generated torque, and power transmitted to the shaft are the same for each of the stages.

The basic design of a turbodrill stage is shown in Fig. 3. In stator and rotor, the drilling fluid flows between two coaxial cylindrical layer with diameter D_2 and D_5 . The simplest approach for turbine analysis is to assume that the flow conditions at a mean radius, called the pitchline, represent the flow at all radii Dixon and hall (2010). As a result, in order to facilitate the process of design, the diameter of D_{cp} cylinder layer is defined as characteristic cylinder layer with the average flow conditions.

The well-known method of building velocity triangles (and polygons) is used when designing the blade unit profile (see Fig. 4). This method is useful for visualizing changes in the magnitude and direction of the fluid flow due to its interaction with

the blade system. Fluid enters the stator with an absolute velocity c_1 and at an absolute velocity angle α_1 and accelerates to an absolute velocity c_2 at angle α_2 . All angles are measured from the axial direction (x). From the velocity diagram, the rotor inlet relative velocity w_2 , at a relative velocity angle β_2 , is found by subtracting, vectorially, the blade speed, U , from the absolute velocity c_2 . The relative flow within the rotor accelerates to velocity w_3 at an angle β_3 at rotor outlet. The analysis of the flow-field within the rotating blades of a turbodrill is performed in a frame of reference that is stationary relative to the blades. In this frame of reference the flow appears as steady, whereas in the absolute frame of reference it would be unsteady. This makes any calculations significantly more straightforward and therefore relative velocities and relative flow quantities are used in this study.

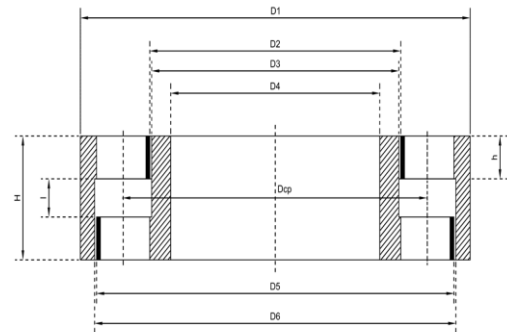


Fig. 3. Schematic of Turbodrill stage geometry, after Eskin and Maurer (1997).

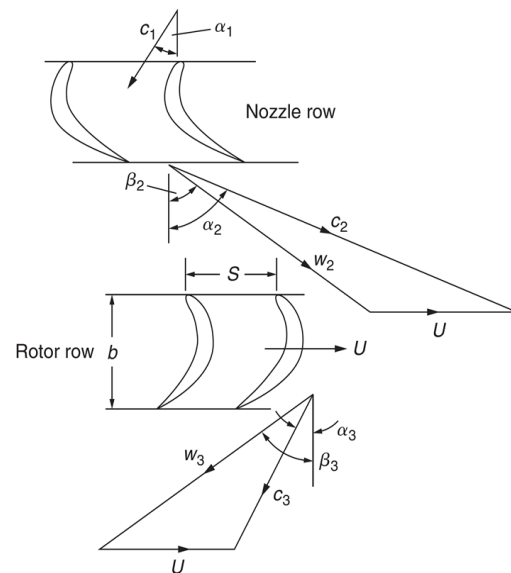


Fig. 4. Turbine Stage Velocity Diagrams, Dixon and Hall (2010).

Three key non-dimensional parameters are related to the shape of the turbine velocity triangles and are used in fixing the preliminary design of a turbine stage. These are described in the following sections.

3.1 Design Flow Coefficient

Design flow coefficient is defined as the ratio of the meridional flow velocity to the blade speed, $\phi=c_m/U$, Dixon and hall (2010). In general, the flow in a turbomachine has components of velocity along all three cylindrical axes (axial x , radial r , and tangential r_θ axes). However, for turbodrill as an axial turbomachinery, to simplify the analysis it is usually assumed that the flow does not vary in the tangential direction. In this case, the flow moves through the machine on axi-symmetric stream surfaces. The component of velocity along an axi-symmetric stream surface is called the meridional velocity (c_m), expressed as:

$$c_m = \sqrt{c_x^2 + c_r^2} . \quad (6)$$

As a result, in purely axial-flow machines such as turbodrill, the radius of the flow path is constant and therefore, the radial flow velocity will be zero and $c_m=c_x$. Therefore, the flow coefficient for turbodrill is defined as:

$$\phi = \frac{c_x}{U} . \quad (7)$$

The value of ϕ for a stage determines the relative flow angles. A stage with a low value of ϕ implies highly staggered blades and relative flow angles close to tangential axis, whereas high values imply low stagger and flow angles closer to the axial axis, Dixon and hall (2010).

3.2 Stage Loading Coefficient

The stage loading is defined as the ratio of the stagnation enthalpy change through a turbine stage to the square of the blade speed, $\psi=\Delta h_0/U^2$. In turbodrill that is assumed to be an adiabatic turbine, the stagnation enthalpy change is equal to the specific work, ΔW , and because it is a purely axial turbine with constant radius, we can use the Euler work equation ($\Delta W=U \times \Delta c_\theta$) to write, $\Delta h_0=U \times \Delta c_\theta$, Dixon and hall (2010). As a result, the stage loading for turbodrill can be written as:

$$\psi = \frac{\Delta c_\theta}{U} , \quad (8)$$

where Δc_θ represents the change in the tangential component of absolute velocity through the rotor. Thus, high stage loading means large flow turning and leads to highly “skewed” velocity triangles to achieve this turning. Since the stage loading is a non-dimensional measure of the work extraction per stage, a high stage loading is desirable because it means fewer stages needed to produce a required work output, Dixon and hall (2010). As a result, with designing blades leading to large flow turning, the stage loading coefficient will be higher and smaller turbodrill with lesser stages can result to the required power as long as being limited by the effects that high stage loadings have on efficiency.

3.3 Stage Loading Coefficient

The stage reaction is defined as the ratio of the static enthalpy drop in the rotor to the static

enthalpy drop across the turbine stage, Dixon and hall (2010):

$$R = \frac{h_2 - h_3}{h_1 - h_3} . \quad (9)$$

Taking the flow through a turbodrill as isentropic, the equation of the second law of thermodynamics, $Tds=dh-dp/\rho$ can be approximated by $dh=dp/\rho$, and ignoring compressibility effects, the reaction can thus be obtained as, Dixon and hall (2010):

$$R = \frac{p_2 - p_3}{p_1 - p_3} . \quad (10)$$

The reaction therefore indicates the drop in pressure across the rotor compared to that of the stage. It describes the asymmetry of the velocity triangles and is therefore a statement of the blade geometries, Dixon and hall (2010). For example, a 50% reaction turbodrill implies velocity triangles that are symmetrical, which leads to similar stator and rotor blade shapes. Typically, in prior turbodrills design a 50% reaction was selected (i.e. the stator blades and the rotor blades are symmetric), Natanael et al. (2008). In contrast, a zero reaction turbodrill stage means a little pressure change through the rotor. This requires rotor blades that are highly cambered, that do not accelerate the relative flow greatly, and low cambered stator blades that produce highly accelerating flow. Axial thrust resulting from the reaction on the rotor blade is typically absorbed by thrust bearings. A higher reaction typically increases the thrust created by the rotor vane, which must then be absorbed by thrust bearings. By significantly reducing the amount of axial thrust absorbed by the thrust bearings, the friction in the thrust bearings can be reduced, thereby decreasing resistance to rotation of the shaft and increasing the efficiency of the turbodrill as a whole.

4. PRELIMINARY TURBODRILL STAGE DESIGN

The process of designing the best turbodrill for a given application involves juggling several parameters that may be of equal importance. In consequence, a simple presentation can hardly do justice to the real problem of an integrated design. The main goal in the preliminary stage design of a turbodrill is to fix the shapes of the velocity triangles, either by setting the flow angles or by choosing values for the three dimensionless design parameters, ϕ , ψ , and R .

In normal multistage turbodrill, with identical mean velocity triangles for all stages, the axial velocity and the mean blade radius must remain constant throughout the turbodrill, therefore $c_x=c_m=\text{constant}$, $a_1=a_2$, and we have:

$$r_m = r_{rms} = \sqrt{\frac{r_{sh}^2 + r_h^2}{2}} . \quad (11)$$

From the specification of the turbodrill, the design will usually have a known mass flow rate of the

drilling fluid and a required power output. As a result, the specific work per stage can be determined from the stage loading and the blade speed and, consequently, the required number of stages can be found as following:

$$n_{stage} \geq \frac{\Delta W}{\psi U^2}. \quad (12)$$

An inequality is used in this equation, because the number of stages must be an integer value. The equation here shows how a large stage loading can reduce the number of stages required in a multistage turbodrill. Also it shows that a high blade speed, U , is desirable as it will reduce the number of required stages.

For turbodrills, several useful relationships can be derived relating the shapes of the velocity triangles to the three dimensionless design parameters. These relationships are important for the preliminary design. Starting with the definition of the stage reaction, and accepting no work is done through the stator, so the stagnation enthalpy remains constant across it and after proper substitutions, finally the relations between flow coefficients and angles are obtained as following:

$$R = \frac{\phi}{2}(\tan \beta_3 - \tan \beta_2) = 1 - \frac{\phi}{2}(\tan \alpha_2 - \tan \alpha_1) \quad (13)$$

Also it can be obtained that:

$$\psi = 2(1 - R + \phi \tan \alpha_1). \quad (14)$$

Two important angles in the geometry of a rotor vane are β_2 and β_3 . These two angles are important factors in the performance of the rotor vane because they determine the change in the direction of the drilling fluid passing through the rotor blade. β_2 plus β_3 is preferably less than 120 degree to avoid excessive blade turning, which can damage the rotor vanes, Natanael *et al.* (2008).

To determine β_2 and β_3 from Eq. (13) we can write:

$$R = \frac{c_x}{2U}(\tan \beta_3 - \tan \beta_2). \quad (15)$$

then,

$$\beta_3 = \tan^{-1}\left(\frac{2UR}{c_x} + \tan \beta_2\right). \quad (16)$$

Also the work done on the rotor by unit mass of fluid, the specific work, equals the stagnation enthalpy drop incurred by the fluid passing through the stage and according to the Euler work equation this can be written mathematically as:

$$\Delta W = \Delta h_0 = U\Delta c_\theta = U c_x(\tan \beta_2 + \tan \beta_3). \quad (17)$$

The output power of each stage is obtained as following:

$$P = \rho Q \Delta W = \rho Q U c_x(\tan \beta_2 + \tan \beta_3). \quad (18)$$

Also the output torque of each stage is:

$$T = \rho Q r_m c_x(\tan \beta_2 + \tan \beta_3). \quad (19)$$

Solving for β_3 results in:

$$\beta_3 = \tan^{-1}\left(\frac{P}{\rho Q U c_x} - \tan \beta_2\right). \quad (20)$$

Equations (16) and (20) can be combined to solve for β_2 . This yields:

$$\beta_2 = \tan^{-1}\left(\frac{P}{2\rho Q U c_x} - \frac{UR}{c_x}\right). \quad (21)$$

The fluid exiting from the stator vane should leave with a close angle to the inlet angle β_2 of the rotor vane. This helps in avoiding an abrupt direction change of the fluid, which can result in the fluid separation on the rotor vane. Fluid separation results in energy losses that increase the load on the pumps, while not providing rotational force to rotate the rotor. Fluid separation also occurs at the trailing edges of the stator and rotor vanes, Natanael *et al.* (2008).

After calculating β_2 and β_3 , a stagger angle (ζ) can be determined that is the angle between the chord line and the axial flow direction. After determining the stagger angle, the ideal length of the chord can be calculated based on the angle and desired length of the rotor vane. With the basic profile of the rotor vane determined, the stator exit angle can be calculated. The stator exit angle, α_2 , may be selected to be substantially similar to the rotor inlet swirl angle and is calculated as:

$$\alpha_2 = \tan^{-1}\left(\frac{c_x \tan \beta_2 + U}{c_x}\right). \quad (22)$$

With the profile of the stator and rotor vanes being defined, an optimum number of blades per stator and rotor and the chord lengths of the blades can also be estimated during the preliminary design. The aspect ratio of a blade row is the height, or blade span, divided by the axial chord, H/b . A suitable value of this is set by mechanical and manufacturing considerations and will vary between applications. Typically, in prior turbodrills design the aspect ratio for rotor blades was 0.5. It has been found that energy losses may be reduced by increasing the aspect ratio of the stator and/or rotor blades, Natanael *et al.* (2008). To find the ratio of blade pitch to axial chord, S/b , the Zweifel criterion for blade loading can be applied. The Zweifel criterion states that for turbine blades there is an optimum space-chord ratio that gives a minimum overall loss. Typically, the Zweifel criterion, Z , is assumed to be between 0.5 and 1.2, Dixon and Hall (2010). If the spacing between the blades is made small, the fluid receives the maximum amount of guidance from the blades, but the friction losses will be large. On the other hand, with the same blades spaced well apart, friction losses are small but, because of poor fluid guidance, the losses resulting from flow separation are high, Dixon and Hall (2010).

For a known axial chord, knowing S/b fixes the number of blades on each stator and rotor row as, Dixon and Hall (2010):

$$N_B = \frac{4\pi r_m \times \cos^2 \beta_3 (\tan \beta_2 + \tan \beta_3)}{Z \times b} \quad (23)$$

While it is common to have the same number of blades per rotor and stator, it is worth to examine various numbers of blades on the rotor and stator and check the performance with computational fluid dynamics (CFD) simulations.

5. NUMERICAL SIMULATIONS

In this study with the objective of fluid flow simulations through small diameter turbodrill suitable for CT Turbodrilling system, ANSYS 14.0 TurboSystem tools together with ANSYS CFX were utilized to investigate the turbodrill performance with different mass flow rates of pure water, air and mist running in various rotation speeds. Here, the objective is to increase optimized output power and rotation speed suitable for hard rocks CT Turbodrilling system to reach higher drilling rates.

5.1 Geometry and Meshing

The shroud (housing) and hub (shaft) diameters of the turbodrill for the applications of this study were set to be 5 and 2.6 cm, respectively. Consequently, the spanwise height (H) will be 1.2 cm for this model with no shroud tip between blade tip and housing, i.e. the blades are connected to the housing. The axial chord is 1.5 cm with 14 blades on both stator and rotor rows. Fig. 5 shows the geometry model of the one stage turbodrill prepared for the simulation which is shown here without housing for better illustration.

After building the geometry of the blades row on the stator and rotor, a three-dimensional high quality hexahedral mesh with mesh resolution of about 1×10^6 numbers of hexahedral elements for the domain (one blade of stator and rotor interacting together) was generated to obtain high quality output simulation results. The boundary layer is resolved to ensure a near-wall y^+ of less than 1 to comply with wall function constraints. Figure 6 shows the blade to blade view of the high quality mesh for the stator at mid-span.

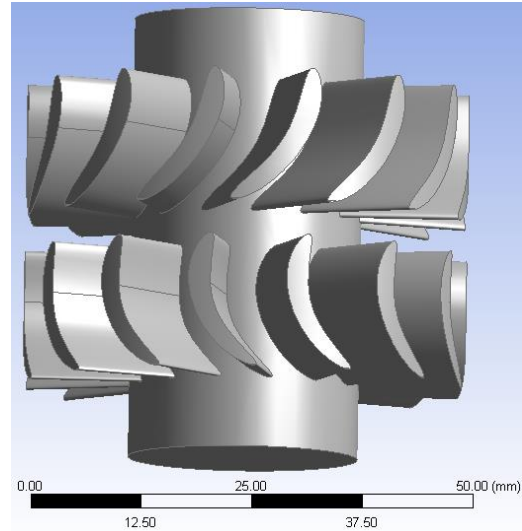


Fig. 5. Geometry model of the one stage turbodrill prepared for the simulation.

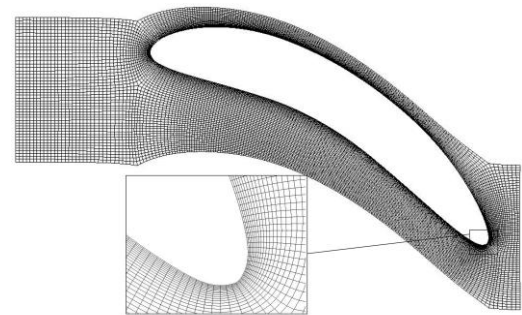


Fig. 6. Blade to blade view of the high quality hexahedral mesh for the stator at the mid-span.

5.2. Physics Definition and Governing Equations

In this study the flow field is calculated based on the Reynolds-Averaged Navier–Stokes (RANS) equations which are derived from the governing Navier–Stokes equations by decomposing the total relevant flow variables into a mean quantity (time-averaged component) and fluctuation component (i.e. for velocity, $u=U+u'$). Here, time-averaged RANS equations, supplemented with two turbulence models of the $k-\epsilon$ (k -epsilon) for water and shear stress transport (SST) which uses a combination of the $k-\epsilon$ and $k-\omega$ (k -omega) for air and mist flow have been used in CFD simulations. Substituting the averaged quantities into the original Navier–Stokes transport equations results in the RANS equations given below in tensor notation:

$$\frac{\partial \rho}{\partial t} + \frac{\partial}{\partial x_j} (\rho U_j) = 0 \quad (24)$$

$$\frac{\partial \rho U_i}{\partial t} + \frac{\partial}{\partial x_j} (\rho U_i U_j) = -\frac{\partial p}{\partial x_i} + \frac{\partial}{\partial x_j} (\tau_{ij} - \rho \overline{u_i u_j}) + S_M \quad (25)$$

where τ_{ij} is the stress tensor (including both normal and shear components of the stress) defined as below:

$$\tau_{ij} = \mu \left(\frac{\partial U_i}{\partial x_j} + \frac{\partial U_j}{\partial x_i} \right) - \rho \overline{u'_i u'_j}. \quad (26)$$

The Reynolds averaged energy equation in tensor notation is:

$$\begin{aligned} \frac{\partial \rho h_{tot}}{\partial t} - \frac{\partial p}{\partial t} + \frac{\partial}{\partial x_j} (\rho U_j h_{tot}) &= \frac{\partial}{\partial x_j} \left[\lambda \frac{\partial T}{\partial x_j} - \rho \overline{u_j h} \right] \\ + \frac{\partial}{\partial x_j} \left[U_i (\tau_{ij} - \rho \overline{u_i u_j}) \right] &+ S_E, \end{aligned} \quad (27)$$

where, h_{tot} is the total enthalpy, related to the static enthalpy, h , by $h_{tot} = h + 0.5 U^2$.

For an incompressible Newtonian fluid (i.e. for pure water), the RANS equations are expressed in tensor notation as following:

$$\rho \frac{\partial U_i}{\partial t} + \rho U_j \frac{\partial U_i}{\partial x_j} = \rho \bar{f}_i + \frac{\partial}{\partial x_j} \left[-p \delta_{ij} + 2\mu \bar{S}_{ij} - \rho \overline{u'_i u'_j} \right], \quad (28)$$

where f_i is a vector representing external forces and δ_{ij} is the Kronecker delta function ($\delta_{ij}=1$ if $i=j$ and $\delta_{ij}=0$ if $i \neq j$). Also, S_{ij} is the mean rate of strain tensor:

$$\bar{S}_{ij} = \frac{1}{2} \left(\frac{\partial U_i}{\partial x_j} + \frac{\partial U_j}{\partial x_i} \right). \quad (29)$$

Here for the mist simulations (mixture of air as continuous phase and water droplets as dispersed fluid particle), a Lagrangian Particle Tracking multiphase model has been used. This particle transport model is capable of modeling dispersed phases which are discretely distributed in a continuous phase. The modeling involves the separate calculation of each phase with source terms generated to account for the effects of the particles on the continuous phase. Also the separated flow analysis method was used in which each particle represents a sample of particles that follow an identical path. The behavior of the tracked particles is used to describe the average behavior of the dispersed phase. The actual number of particles modeled by the representative particle is called the Particle Number Rate. The particle number rate is determined from the mass flow rate assigned to the representative particle divided by the mass of an actual particle.

Here, the objective of using mist as drilling fluid is to add some amount of water to the pumped air to provide cooling to the down hole tools and especially to provide sufficient cooling to the impregnated diamond bit which is cutting the rock by grinding action and produce a large amount of head on bit face. The large surface area of the small water droplets leads to high evaporation rates which extract large amounts of heat. In addition, as the water droplets are converted to steam they expand approximately 1700 times.

In this study, the liquid particle and gas phases were modeled as fully coupled, due to the relatively significant mass of water that interacts with the gas phase; that is, the momentum transfers from

particles to gas, and from gas to particles, were resolved. The choice of one-way or full coupling for particles depends on the mass loading, that is, the ratio of the mass flow rate of particles to the mass flow rate of fluid. One-way coupling may be an acceptable approximation in flows with low mass loadings where particles have a negligible influence on the fluid flow. If the particles influence the fluid flow significantly, then full coupling should be used. The particle source terms acting on the fluid phase are proportional to the particle number rate and the convergence of a simulation can be improved if a sufficiently large number of particles are tracked. Full coupling requires that the particle source terms are included in the continuous phase momentum equations. The momentum sources could be due to turbulent dispersion forces or drag forces.

Particle drag was modeled using the Schiller-Naumann drag model for sparsely distributed, small, and spherical particles. Interphase heat transfer was modeled with Ranz-Marshall correlations which are good for spherical particles. The heat transfer option was set to Total Energy for air (continuous phase) and to Particle Temperature for water particles. The turbulence model used here in a particle tracking simulations only applies to the continuous phases. Turbulence can affect the particles through the particle dispersion force, but the particles can have no effect on the turbulence of the continuous phase, other than indirectly by affecting the velocity field.

The parallel and perpendicular restitution coefficients describe the action of particles when they hit a wall. Coefficient values of 1 described an elastic collision, while values less than 1 describe an inelastic collision. The parallel coefficient will almost always be 1. The perpendicular coefficient will depend on the particle material. Particles that bounce off walls will have a perpendicular coefficient close to 1, while particles that stick to walls will have a perpendicular coefficient of 0. Here, only a few simulation results were included in which both of the restitution coefficients were set equal to 1 for all walls in the domain.

The physical mechanisms by which small particles are transported by a turbulent fluid flow are complex. Here, the particle tracking is carried out by forming a set of differential equations in time for each particle, consisting of equations for position, velocity, temperature, and masses of species. These equations are then integrated using integration methods to calculate the behavior of the particles as they traverse the flow domain. Here, the particle displacement is calculated using forward Euler integration of the particle velocity over timestep (δt). The particle displacement is given as:

$$x_p^n = x_p^o + U_p^o \delta t \quad (30)$$

where the superscripts o and n refer to old and new values respectively, and U_p^o is the initial particle velocity. In forward integration, the particle velocity calculated at the start of the timestep is assumed to remain constant over the entire step. At

the end of the timestep, the new particle velocity is calculated using the analytical solution to the particle momentum equation:

$$m_p \frac{dU_p}{dt} = F_{all}, \quad (31)$$

where F_{all} is the sum of all forces acting on a particle. In this study, considering a discrete particle traveling in a continuous fluid medium, three important forces acting on the particle that affect the particle acceleration are drag force, buoyancy force and forces due to domain rotation (centripetal and Coriolis forces). Therefore, it results at:

$$m_p \frac{dU_p}{dt} = F_D + F_B + F_R, \quad (32)$$

where,

F_D = drag force acting on the particle,

F_B = buoyancy force due to gravity,

F_R = forces due to domain rotation (centripetal and Coriolis forces).

For spherical particle used here, the particle mass can be obtained as:

$$m_p = \frac{\pi}{6} d_p^3 \rho_p. \quad (33)$$

The aerodynamic drag force on a particle is proportional to the slip velocity, U_s , between the particle and the fluid velocity, resulting at following equation, ANSYS (2011):

$$F_D = \frac{1}{2} C_D \rho_F A_F |U_s| U_s, \quad (34)$$

where $U_s = U_f - U_p$ and C_D is the drag coefficient and A_F is the effective particle cross section. The particle momentum source due to drag is calculated from the following equation, ANSYS (2011):

$$\frac{dS}{dt} = -F_D = -\frac{1}{2} C_D \rho_F A_F |U_s| U_s. \quad (35)$$

The source, S , added to the continuous phase is then multiplied with the number rate for that particle.

The buoyancy force is the force on a particle immersed in a fluid. The buoyant force is equal to the weight of the displaced fluid and is given by:

$$F_B = (m_p - m_f)g = m_p \left(1 - \frac{\rho_f}{\rho_p}\right)g = \frac{\pi}{6} d_p^3 (\rho_p - \rho_f)g \quad (36)$$

where g is the gravity vector.

In a rotating frame of reference, the rotation term is an intrinsic part of the acceleration and is the sum of Coriolis and centripetal forces, ANSYS (2011):

$$F_R = m_p (-2 \Omega \times U_p - \Omega^2 \times r_p), \quad (37)$$

where, Ω is the angular velocity and r_p is the particle distance with the axis of rotation.

In turbulent tracking, the instantaneous fluid velocity is decomposed into mean, \bar{v}_f , and fluctuating, v'_f , components. The particle trajectories are not deterministic here and two identical particles, injected from a single point, at different times, may follow separate trajectories due to the random nature of the instantaneous fluid velocity. It is the fluctuating component of the fluid velocity which causes the dispersion of particles in a turbulent flow, ANSYS (2011). The model of turbulent dispersion of particles that is used in ANSYS CFX, assumes that a particle is always within a single turbulent eddy. Each eddy has a characteristic fluctuating velocity, v'_f , lifetime, τ_e , and length, l_e . When a particle enters the eddy, the fluctuating velocity for that eddy is added to the local mean fluid velocity to obtain the instantaneous fluid velocity. The turbulent fluid velocity, v'_f , is assumed to remain as long as the particle/eddy interaction time is less than the eddy lifetime and/or the displacement of the particle relative to the eddy is less than the eddy length. If either of these conditions is exceeded, the particle is assumed to be entering a new eddy with new characteristic v'_f , τ_e and l_e , ANSYS (2011). The turbulent velocity, eddy length and lifetime are calculated based on the local turbulence properties of the flow as following, ANSYS (2011):

$$v'_f = \Gamma(2k/3)^{0.5}, \quad (38)$$

$$l_e = \frac{C_\mu^{3/4} k^{3/2}}{\varepsilon}, \quad (39)$$

$$\tau_e = l_e / (2k/3)^{0.5}, \quad (40)$$

where k and ε are the local turbulent kinetic energy and dissipation, respectively, and C_μ is a turbulence constant. The factor $C_\mu^{3/4}$ was chosen to relate the characteristic length scale to the eddy dissipation length. The variable Γ is a normally distributed random number which accounts for the randomness of turbulence about a mean value.

In this study, the equations of motion of individual particles are solved without considering collisions between particles and as a result the presence of other particles is not taken into account.

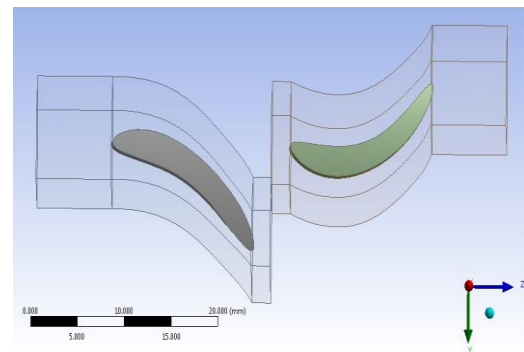


Fig. 7. Blade to blade view of the model.

In this paper, because of the periodic symmetry between the blades on stator row and also on rotor row and having the same number of blades on each row, i.e. pitch ratio of 1, the simulations were conducted for one blade of stator and one blade of rotor interacting with each other. Figure 7 shows the blade to blade view of the model. The results will show velocity vectors at 50% span between hub and shroud and pressure profiles on the meridional view of the flow passage.

6. SIMULATION RESULTS

In overall, the simulation results show that the turbodrill performance is highly dependent on the mass flow rate of the drilling fluid. As the mass flow rate is increased the expected optimum rotation speed and output power of the turbodrill increases. While the mass flow rate of the drilling fluid reduces, the output rotation speed, the power and consequently the shaft torque will drastically decrease to allow the velocity vectors entering rotor be aligned with the rotor inlet angle (to be effective in producing rotational effects on the rotor blades). Figures 8 to 10 show the CFD simulation results for water and with 6 Kg/s of mass flow rate and with three different rotation speeds of 2, 3 and 4 thousand revolutions per minute (rpm). Figures 11 to 13 show the CFD simulation results for water and with 7 Kg/s of mass flow rate and with three different rotation speeds of 3, 4 and 5 thousand

rpm. For water, due to limitations on the mass flow rates that can be injected from the surface pump down through the CT assembly to bottom hole to actuate the turbodrill (having huge pressure losses through the drilling assembly), the practical mass flow rates for this small size CT assembly should be below 7 Kg/s, and here with the mass flow rate of 7 Kg/s, optimum rotation speed is below 4,000 rpm and is around 3,000 rpm. Table 1 shows the CFD simulation results for one stage proposed turbodrill model for the two water mass flow rates of 6 and 7 Kg/s.

Figure 14 shows the output power and torque trends from the simulation results versus rotation speed (rpm) for the two water mass flow rates of 6 and 7 Kg/s. The simulation results show a very good match for the proposed turbodrill model. With this chart, the resulted power and torque in any other rotation speeds can be obtained with a very good accuracy. For more illustration and comparison, the basic performance characteristics for a turbine down hole motor (with 17 cm outer diameter) are shown in Fig. 15 for a constant flow rate. For a specific weight of 1.5 SG of the drilling fluid (mud) system the torque/speed relationship and the corresponding power output are shown by solid lines. In this example to generate the optimum mechanical output power, the turbine has to be operated at the maximum efficiency which occurs at a bit speed of about 1,000 rpm.

Table 1 Water Simulation Results for one stage for the two mass flow rates of 6 and 7 Kg/s.

| Speed (rpm) | Power (W) | | Torque (N.mm) | |
|-------------|-----------|--------|---------------|---------|
| | 6 Kg/s | 7 Kg/s | 6 Kg/s | 7 Kg/s |
| 100 | 12.82 | 17.67 | 1224.56 | 1687.17 |
| 1000 | 106.95 | 151.96 | 1021.41 | 1451.17 |
| 2000 | 166.06 | 249.06 | 792.94 | 1189.28 |
| 3000 | 175.55 | 291.39 | 558.83 | 927.58 |
| 4000 | 128.71 | 262.44 | 307.29 | 626.58 |
| 5000 | 5.2 | 159.24 | 9.93 | 304.16 |
| 6000 | | 20.85 | | 33.19 |

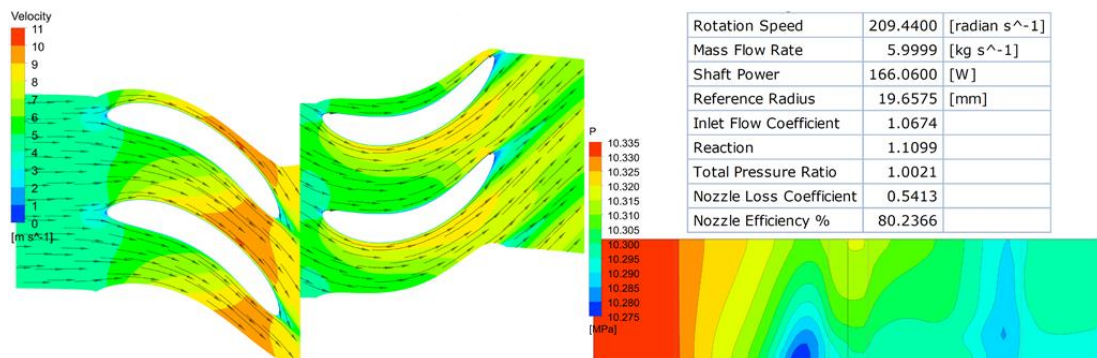


Fig. 8. Water flow simulation results with mass flow rate of 6 Kg/s and rotation speed of 2,000 rpm.

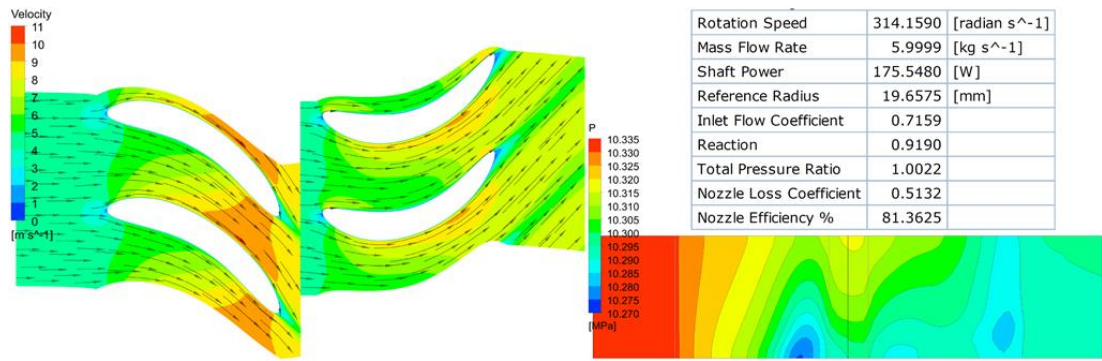


Fig. 9. Water flow simulation results with mass flow rate of 6 Kg/s and rotation speed of 3,000 rpm.

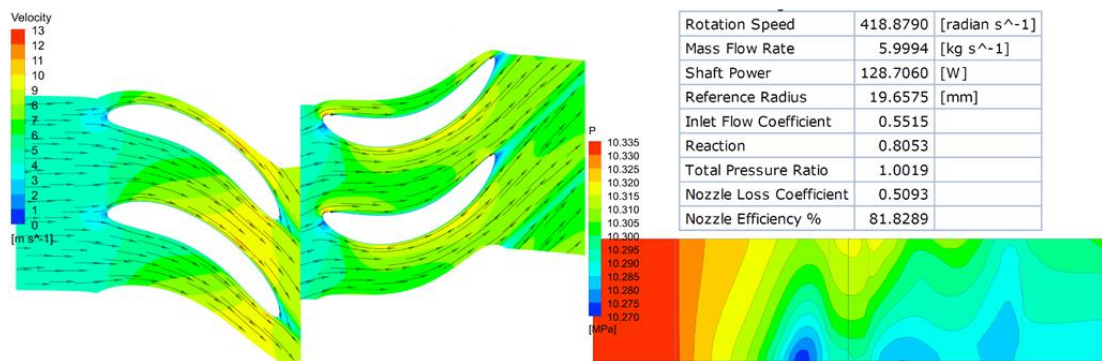


Fig. 10. Water flow simulation results with mass flow rate of 6 Kg/s and rotation speed of 4,000 rpm.

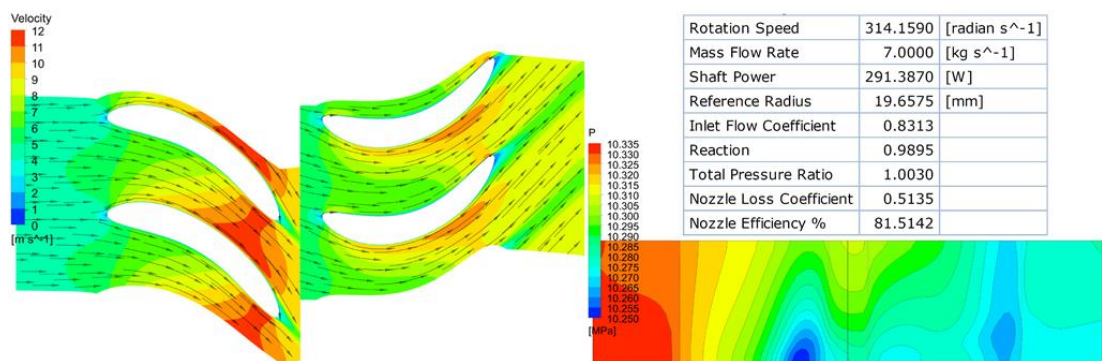


Fig. 11. Water flow simulation results with mass flow rate of 7 Kg/s and rotation speed of 3,000 rpm.

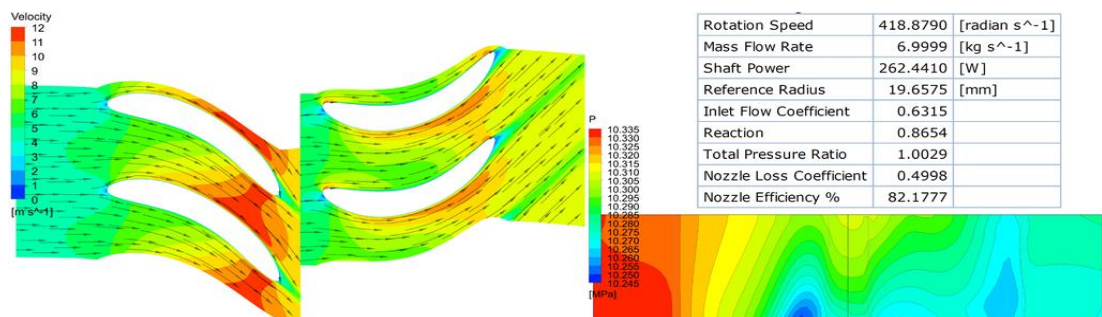


Fig. 12. Water flow simulation results with mass flow rate of 7 Kg/s and rotation speed of 4,000 rpm.

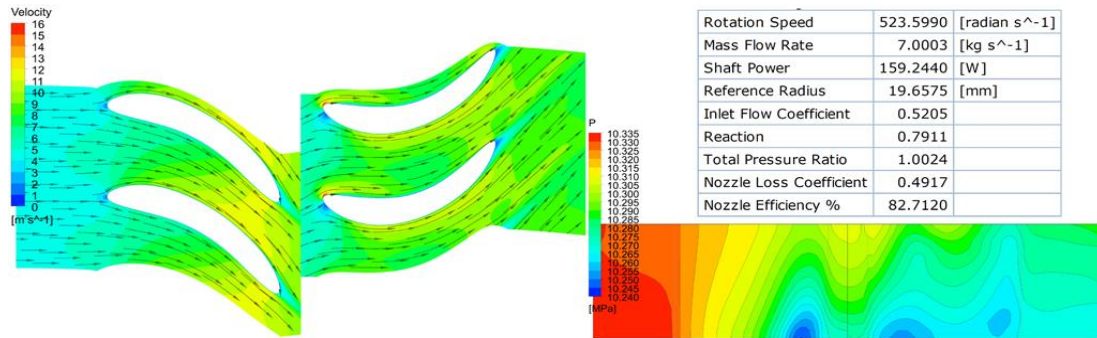


Fig. 13. Water flow simulation results with mass flow rate of 7 Kg/s and rotation speed of 5,000 rpm.

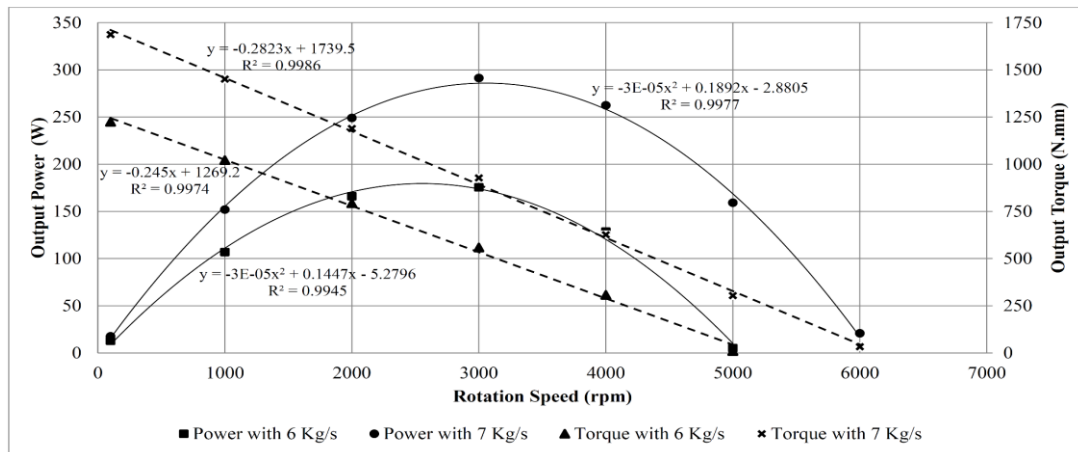


Fig. 14. Water simulation results of one stage proposed turbodrill for the two mass flow rates of 6 and 7 Kg/s with different rotation speeds.

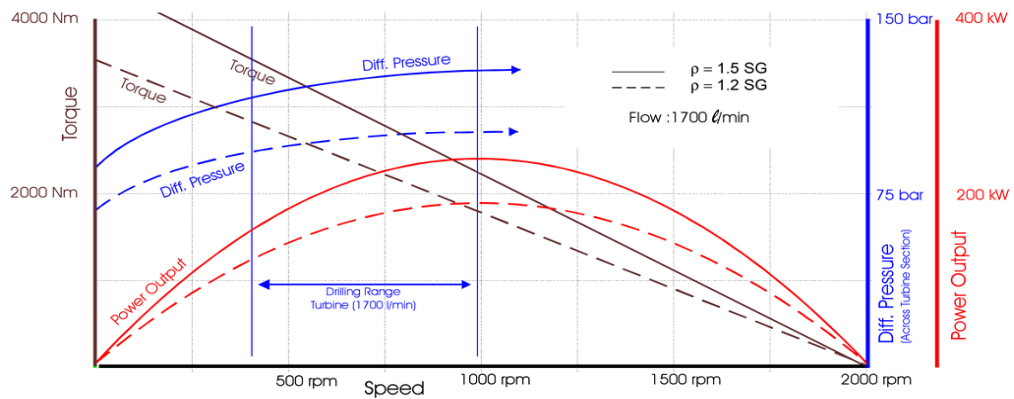


Fig. 15. Turbodrill performance characteristics versus Mud Weight, Reich et al. (2000).

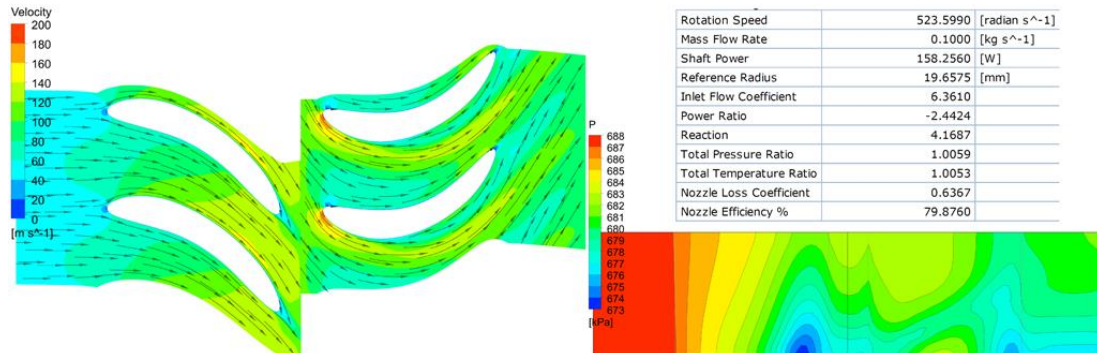


Fig. 16. Air flow simulation results with mass flow rate of 0.1 Kg/s, and rotation speed of 5,000 rpm.

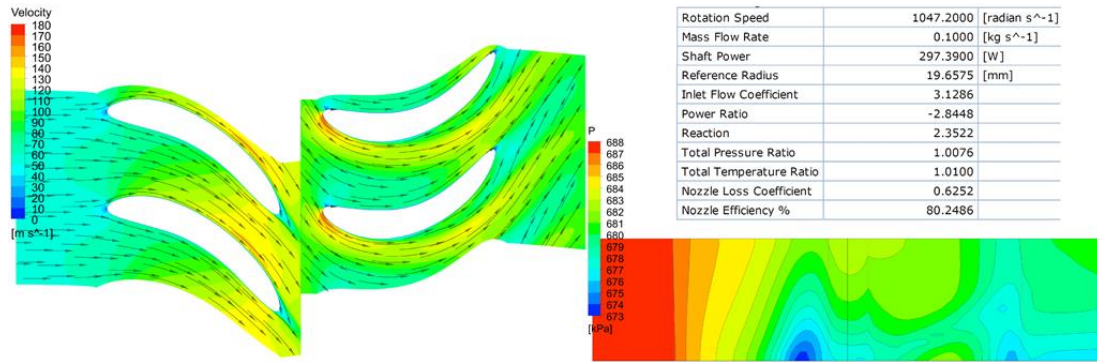


Fig. 17. Air flow simulation results with mass flow rate of 0.1 Kg/s, and rotation speed of 10,000 rpm.

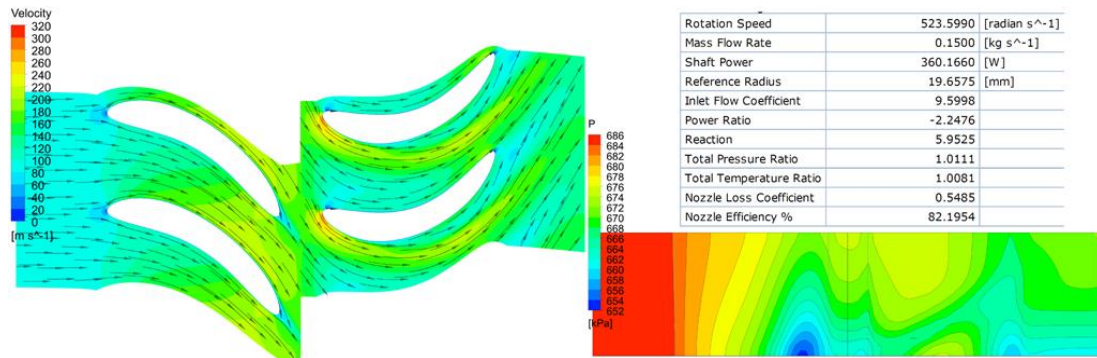


Fig. 18. Air flow simulation results with mass flow rate of 0.15 Kg/s, and rotation speed of 5,000 rpm.

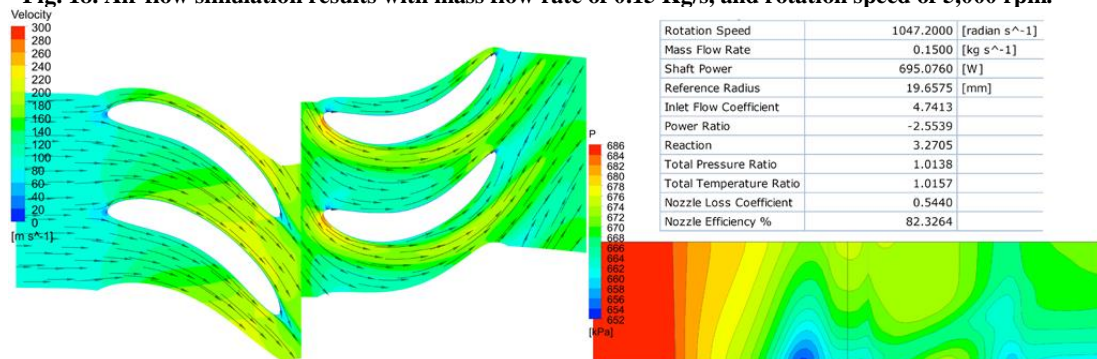


Fig. 19. Air flow simulation results with mass flow rate of 0.15 Kg/s, and rotation speed of 10,000 rpm.

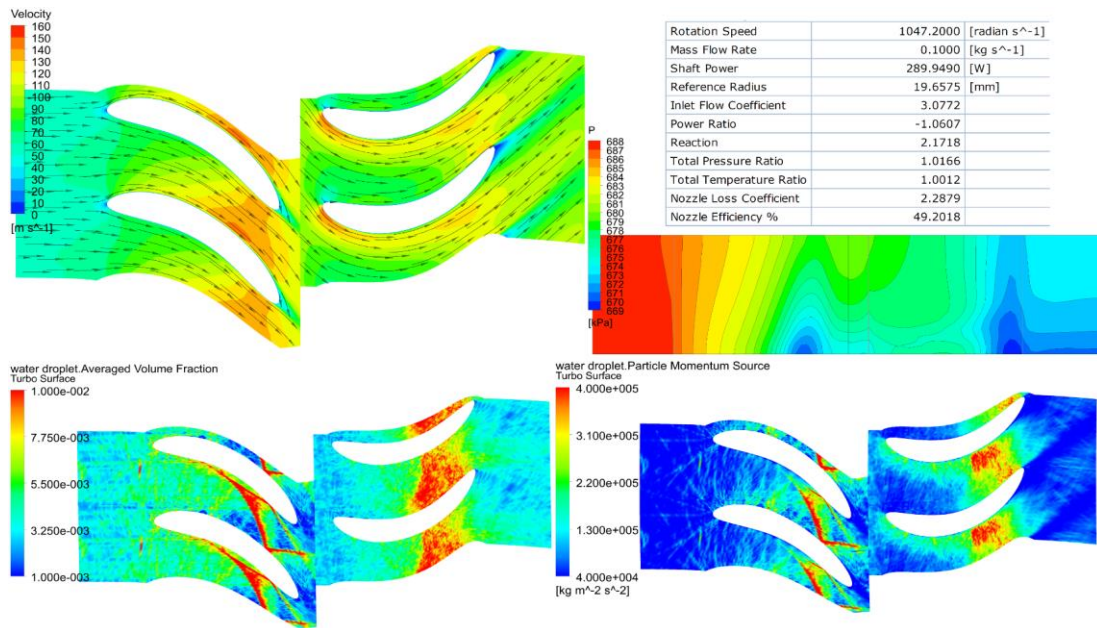


Fig. 20. Two phase flow (mist) simulation of air (0.1 Kg/s) and water droplets (0.2 Kg/s) with speed of 10,000 rpm.

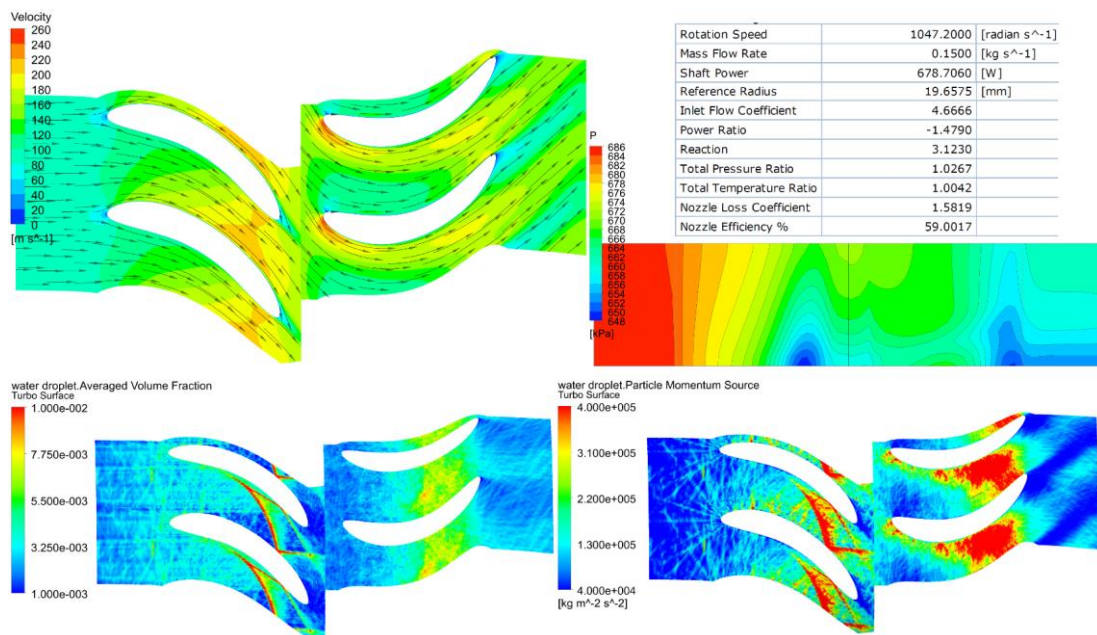


Fig. 21. Two phase flow (mist) simulation of air (0.15 Kg/s) and water droplets (0.2 Kg/s) with speed of 10,000 rpm.

Figures 16 and 17 show the simulation results for air flow with 0.1 Kg/s mass flow rate for 5,000 and 10,000 rpm rotation speed, respectively. Also, Figures 18 and 19 show the simulation results for air flow with 0.15 Kg/s mass flow rate for 5,000 and 10,000 rpm rotation speed, respectively. From these results it is clear that with air, it can be possible to have higher rotation speeds with practical air mass flow rates.

Figures 20 and 21 show the simulation results for the two phase flow (mist) of air as continuous phase and water droplets as dispersed fluid particle with 0.1 and 0.15 Kg/s air mass flow rate, respectively. In both cases 0.2 Kg/s mass flow rate of water

particles are simulated. In each time step about 15,000 particles of water with 0.1 mm specified diameter were injected to the domain in the same temperature with air flow (25 °C). These figures also show the average volume fraction of water particles and particle momentum sources in the blade to blade view of the mid-span.

7. CONCLUSION

Basic design methodology for multistage Turbodrill (turbine down hole motor) optimized for small size Coiled Tube (CT) Turbodrilling system for deep hard rocks mineral exploration applications was presented. The results of numerical simulations for

turbodrill stage performance with asymmetric blades profiles on stator and rotor with different fluid, mass flow rates and rotation speeds were reported.

The simulation results included in this paper for the specific blades configuration showed that the turbodrill performance is highly dependent on the mass flow rate of the drilling fluid, i.e. as the mass flow rate increases the expected rotation speed of the turbodrill and consequently the output power and torque will increase. Also, for a given range of rotation speeds and drilling fluid mass flow rates suitable for optimized Turbodrilling system, the turbodrill specifications (blade numbers on each row, inlet and outlet angles, etc.) should be designed specifically in a way that it achieves the maximum possible flow hydraulics energy which in turn provides the desired mechanical power with a high efficiency.

ACKNOWLEDGEMENTS

The authors would like to express their sincere thanks to the Deep Exploration Technologies Cooperative Research Centre (DET CRC) for their financial supports towards this project

REFERENCES

- Calhoun, D. A., C. Helze, and R. J. LeVeque (2008). Logically Rectangular Grids and Finite Volume Methods for PDEs in Circular and Spherical Domains, *Society for Industrial and Applied Mathematics* 50(4), 723–752.
- Chourasia, M. K. and T.K. Goswami (2006). Steady state CFD modeling of airflow, heat transfer and moisture loss in a commercial potato cold store, *International Journal of Refrigeration* 30, 672-689.
- Early (1998). R.E, Technology of Dairy Products, 2nd edition, *Blackie Academic & Professional*, London.
- FAO/WHO (2002). Proposed Draft Revised Standard for Fermented Milks. *Codex Committee on Milk and Milk Products. Doc CX/MMP 02/4 (Jan 2002). Joint FAO/WHO Food Standards Programme*. FAO/WHO, Viale di Caracalla 00100, Rome.
- Gonçalves, B. J., Department of Food Science, *Federal University of Lavras – UFLA, Campus Universitário*, 37200-000 Lavras, Minas Gerais, Brazil.
- Hoang, M. L., P. Verboven, J. De Baerdemaeker, and B. M. Nicolai (2000). Analysis of the air flow in a cold store by means of Computational Fluid Dynamics, *International Journal of Refrigeration* 23 127-140
- Mirade, P. S. and J. D. Daudin (1998), Numerical simulation and validation of the air velocity field in a meat chiller. *International Journal of Applied Science and Computations*; 5(1), 11-24.
- Modi, H. A. (2011). Fermented milk products, *Avishkar Publishers' Distributors*, India.
- Robert H.Perry, Don Green, Perry's chemical engineers handbook, 6th edition, *McGraw- Hill International Editions*.
- Verboven, P. and Nicolai, B. M. Computational Fluid Dynamics- a fresh breeze in engineering and design of food cooling processes, *Preprints of the 18th IFAC World Congress Milano (Italy) August 28*, Belgium.
- Wang, H., S. Toubert (1990). Distributed dynamic modelling of a refrigerated room. *International Journal of Refrigeration*; 13, 214-22.
- Zou, Q. (2002). *A CFD modelling system for air flow and heat transfer in ventilated packing systems during forced- air cooling of fresh produce*, PhD thesis, Massey University.